REPORT DOCUMENTATION PAGE

Form Approved
OMB NO. 0704-0188

1. AGENCY USE ONLY (Leave Blank)	2. REPORT DATE April 20, 1998	3. REPORT TYPE AND DATES COVERED FINAL REPORT - 1 Sep 92 to 31 Aug 96

4. TITLE AND SUBTITLE
Fatigue of Advanced In-Situ Composite Solders

5. FUNDING NUMBERS

DAAL03-92-G-0361

6. AUTHOR(S)
S. M. L. Sastry and K. L. Jerina

7. PERFORMING ORGANIZATION NAME(S) AND ADDRESS(ES)

Washington University
Materials Research Laboratory, Campus Box 1087
One Brookings Drive
St. Louis, MO 63130

8. PERFORMING ORGANIZATION REPORT NUMBER

Supersedes AD-A318 416

9. SPONSORING / MONITORING AGENCY NAME(S) AND ADDRESS(ES)

U. S. Army Research Office
P.O. Box 12211
Research Triangle Park, NC 27709-2211

10. SPONSORING / MONITORING AGENCY REPORT NUMBER

ARO 30689.1-RT-EPS

11. SUPPLEMENTARY NOTES
The views, opinions and/or findings contained in this report are those of the author(s) and should not be construed as an official Department of the Army position, policy or decision, unless so designated by the documentation.

12 a. DISTRIBUTION / AVAILABILITY STATEMENT
Approved for public release; distribution unlimited.

12 b. DISTRIBUTION CODE

13. ABSTRACT (Maximum 200 words)

Solder joints used in surface mount technology experience thermomechanical fatigue due to the mismatches in coefficients of thermal expansion of the electrical component, the printed circuit board, and the solder itself, which during thermal cycles causes the solder joint to undergo shear strains. The purpose of this study was to examine and explain the thermomechanical fatigue damage mechanisms of various types of solder compositions. Shear, creep, low cycle fatigue, and thermomechanical fatigue tests were conducted in this research. The development of cracks through heterogeneously coarsened, Sn-enriched bands was observed in Sn-Pb eutectic and solid solution strengthened alloys failed in thermomechanical fatigue. The dominant damage mechanism for these alloys was determined to be dislocation climb. Dispersion strengthening inhibited heterogeneous coarsening, and resulted in solders with greater thermomechanical fatigue lifetimes.

14. SUBJECT TERMS
solder alloys, solder joints, fatigue, thermomechancal fatigue, creep, fatigue resistant solder

15. NUMBER OF PAGES
45

16. PRICE CODE

17. SECURITY CLASSIFICATION OR REPORT UNCLASSIFIED	18. SECURITY CLASSIFICATION ON THIS PAGE UNCLASSIFIED	19. SECURITY CLASSIFICATION OF ABSTRACT UNCLASSIFIED	20. LIMITATION OF ABSTRACT UL

NSN 7540-01-280-5500
(Rev.2-89)
Prescribed by ANSI Std. 239-18

Standard Form 298

298-102

19980608 012

Fatigue of Advanced In-Situ Composite Solders

FINAL REPORT

by: S. M. L. Sastry, Principal Investigator
and K. L. Jerina

April 20, 1998

ABSTRACT

Solder joints used in surface mount technology experience thermomechanical fatigue due to the mismatches in coefficients of thermal expansion of the electrical component, the printed circuit board, and the solder itself, which during thermal cycles causes the solder joint to undergo shear strains. The purpose of this study was to examine and explain the thermomechanical fatigue damage mechanisms of various types of solder compositions. Shear, creep, low cycle fatigue, and thermomechanical fatigue tests were conducted in this research. The development of cracks through heterogeneously coarsened, Sn-enriched bands, was observed in Sn-Pb eutectic and solid solution strengthened alloys failed in thermomechanical fatigue. The dominant damage mechanism for these alloys was determined to be dislocation climb. Dispersion strengthening was effective in inhibiting heterogeneous coarsening and resulted in solders with greater thermomechanical fatigue lifetimes.

TABLE OF CONTENTS

LIST OF TABLES

LIST OF FIGURES

1. INTRODUCTION

Over the last thirty years the basic through hole technology design of printed circuit boards has been gradually replaced by surface mount technology (SMT). SMT, as shown in Figure 1-1, allows electronic components to be soldered to both sides of a printed circuit board (PCB). This allows for higher chip densities and reduces manufacturing costs.
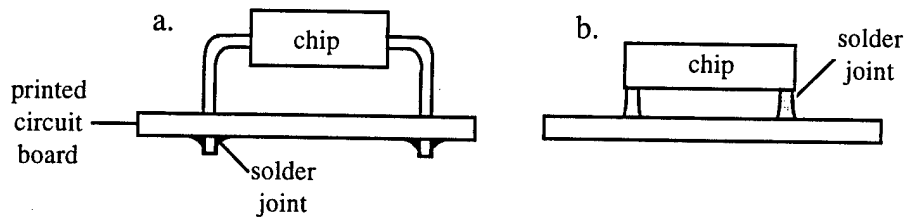
Figure 1-1. Comparison of joint technologies: a.) Through hole, b.) Surface mount

In traditional through hole solder technology the component's pin provided most of the mechanical support for the component while the solder provided the electrical connection to the circuit board. In surface mount technology applications the solder must provide not only an electrical connection but also serve as the sole mechanical attachment between components and the PCB.

Electrical circuits typically experience thermal variations during changes in environment and on-off power cycles. During typical power cycles in electrical components, Joule heating can cause components to thermally cycle from 25 °C to 100 °C [1]. Environmental temperature changes in avionics can results in temperatures varying from -55 °C to 100 °C [2]. Shear forces are applied to solder joints as a result of thermal gradients, due to mismatches in coefficients of thermal expansion between fiberglass printed circuit boards (CTE 17 x 10^{-6} °C^{-1}), electronic components (CTE 6 x 10^{-6} °C^{-1}), and the solder itself (CTE 25 x 10^{-6} °C^{-1}) [3]. Current trends point towards the application of larger silicon devices and multi-chip modules, which will induce larger strains on solder joints [4]. Thus, solder reliability has become an important concern of the electronics industry.

Typical solder used in electronics must have low melting temperatures so that the electronic circuitry and PCBs will not be damaged during reflow of the solder. The most common solder, eutectic Sn-Pb, has a melting temperature of only 183 °C. Room temperature corresponds to 64% of this solder's melting temperature, when expressed in degrees Kelvin. When the typical shear strains caused by thermal expansion are applied to this solder, it will experience thermally activated, time-dependent damage mechanisms such as creep, hardening and softening, and microstructural change, as well as low-temperature, low-cycle fatigue mechanisms. It is possible for a solder joint to experience more than one of these damage mechanisms during each thermal cycle [2,5,6].

The application of both cyclic strains and temperatures to a material is referred to as thermomechanical fatigue (TMF). Material properties such as shear and tensile strengths, low-cycle fatigue results, and creep resistances can be evaluated for solder joints using isothermal conditions. However, these tests usually only analyze the effects of one dominant damage mechanism. Thermomechanical fatigue tests are needed to accurately predict the lifetimes of solder joints in service and to evaluate the effect of the several damage mechanisms which may be operating simultaneously. These tests will result in a better understanding of how different alloys fail during service conditions.

2. LITERATURE REVIEW

Microstructure of Solders

Figure 2-1 shows the phase diagram of the Sn-Pb, which is the most commonly used solder in the electronics industry [8]. The 63 weight % Sn and 37 % weight Pb alloy is usually referred to as the eutectic composition, although the figure shows that the actual eutectic composition is 61.9 wt. % Sn and 38.1 wt.% Pb.
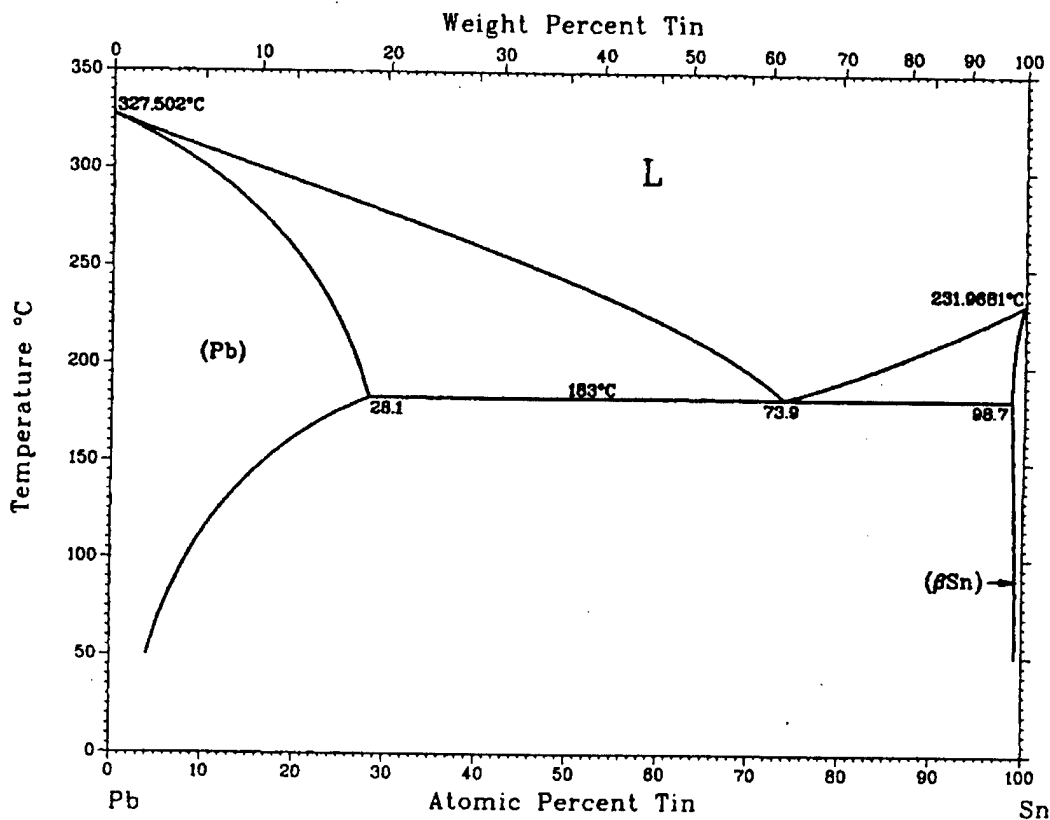
Figure 2-1. Sn-Pb phase diagram [7]

The equilibrium solidification of a eutectic Sn-Pb alloy undergoes the following reaction:

$$\text{Liquid} \rightarrow \alpha\text{-Pb (FCC)} + \beta\text{-Sn (BCT)} \, (2.1)$$
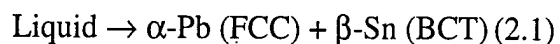
The phase diagram shows that the solubility of Sn in Pb is around 19.2 wt. % at 183 °C, while Pb has a solubility in Sn of only 3.0 %. The solubility of Sn drops considerably with decreasing temperature; at 20 °C the solubility limit for Sn is approximately 2 wt. %. Therefore, a rapid cooling of a reflowed Sn-Pb eutectic solder will result in Pb phases supersaturated with Sn [9].

The microstructure of near eutectic Sn-Pb solder depends on the cooling rates utilized. Slow cooling rates after solder reflow will result in a lamellar arrangement of Pb rich phases in a matrix of Sn, arranged in colonies, with a coarse grain size. Slightly faster cooling rates produce a lamellar structure with smaller grains and finer lamellar structures. Faster cooling rates give rise to a globular or equiaxed structure of Pb phases in a Sn matrix. Actual joints used in electronics display eutectic, globular, and a combination of both microstructures, due to the variety of cooling rates which are used for the different solder processing techniques. [1, 4, 10, 11].

The lamellar eutectic microstructure exhibits larger yield strengths, lower elongations, better creep resistances, and lower strain rate sensitivities than the globular microstructure. These characteristics can be attributed to the difficulties of moving dislocations through a two phase structure with fine spacings, such as the lamellar structure. Solder has been observed to becomes softer as the microstructure becomes less regularly aligned and more globular [11].

One reasonable method to improve the mechanical properties of solder would include altering the processes of manufacturing solder joints to produce lower cooler rates, which would result in solders with a regular lamellar structure. However, there is little motivation for this approach due to the high costs of changing the manufacturing processes currently in use [6].

The as-solidified eutectic structure of 63 wt. % Sn-37 wt. % Pb is not stable at room temperature. The Sn which is initially supersaturated in the Pb phases will decompose, either by precipitates in the Pb phase or by additions to Sn grains if the initial microstructure is fine. Both the Sn and Pb phases will coarsen over time. Because grain growth is a diffusion-controlled process, the rate of coarsening will increase with elevated temperatures and applied strains. The eutectic Sn-Pb solder will slowly coarsen if left at room temperature due to the low melting point (191 °C) of this solder. Room temperature aging of Sn-Pb eutectic solder has been shown to reduce the solder's room temperature shear strength by about 10% [12, 13].

In addition to coarsening, an initially lamellar eutectic Sn-Pb solder which undergoes deformation at an elevated temperate may recrystallize. The microstructure for this solder will become fine grained and equiaxed, with no remnants of the lamellar structure. Research has shown that this type of microstructure displays superplastic characteristics with ductilities of up to 4850% reported. Unfortunately, at the present time it has not

been shown that the superplacticity qualities of the solder can be maintained over time, as the solder tends to coarsen during normal use conditions [8,9,11].

One promising method of strengthening Sn-Pb solders is the addition of properly sized and distributed dispersoids, which have little or no solubility in the Sn or Pb rich phases. These in-coherent particles would strengthen the solder by creating obstacles through which dislocations could not move, effectively impeding the movement of dislocations through the matrix. The additional strengthening expected from dispersion strengthening is given by a modified version of Orowan's equation:

$$\Delta \tau = 1.06 \frac{Gb}{2\pi \ L'} \ln(\frac{x}{\gamma_o}) \quad (2\text{-}2)$$

where b is the Burger's vector, G is the shear modulus of the matrix, x is the dispersoid size, γ_o is the inner cut off radius (usually taken to be equal to 4b), L' is the average spacing of the slip plane, and $\Delta \tau$ is the increase in shear strength due to the addition of dispersions.

The average spacing of the slip plan, represented by L' in equation 2-2, will decrease with larger volume fractions of dispersoids and increase with greater dispersoid sizes. The greatest strengthening from dispersion strengthening will therefore occur with a large volume fraction of very fine dispersoid sizes (typically less than 0.1 µm in diameter) [4, 14].

Dispersion strengthening has been shown to assist in stabilizing the initial solder microstructure from aging effects by restricting grain boundary motion. This type of strengthening is generally more effective than solid solution strengthening in increasing the creep resistance of a matrix. Due to the pinning of dislocations a high threshold stress for creep has been noted with dispersions. In addition, dispersions are effective in blocking dislocation motion at relatively high temperatures (up to 90% of the homologous temperature when expressed in Kelvin) [4, 14, 15].

There are some possible detrimental effects associated with dispersion strengthening. Materials with dispersions often display lower ductility, which tends to result in shorter low cycle fatigue lifetimes. The addition, either by dispersoids or in a solid solution, of ternary particles to the Sn-Pb eutectic can also change the reflow characteristics of the solder, including its wettability and solderability. Altering these properties can result in the production of lower quality joints during electronic solder joint manufacturing, which become expensive to rework by hand [4, 16].

Physical Properties of Bulk Solders

Properties of bulk solders were investigated previously at Washington University by Kuo, and are summarized here [17]. Bulk samples were made by extruding powders of diameters of less than 180 µm into 6 mm rods, which were than machined to produce a

reduced cross section of 3.17 mm. All of these samples were tested under tensile loading conditions.

Tensile tests conducted at a strain rate of 2×10^{-3} s^{-1} indicated that solid solution strengthened solders have yield strengths and ductilities close to that of the eutectic 63 Sn-37 Pb solder. Dispersion strengthened alloys resulted in greater yield strengths, with lower elongations than the solid solution and eutectic solders. Sn-Pb-5 Ni was determined to have the best mechanical properties of the dispersion strengthened alloys tested.

High-cycle (stress controlled) fatigue lives followed the same trend as shown in the tensile tests, with dispersion strengthened alloys giving the longest lifetimes, followed by solid solution strengthened and eutectic compositions. Because the dispersion strengthened alloys have lower ductility they produced the shortest lifetimes in low cycle (strain controlled) fatigue tests. The solid solution strengthened alloys had the longest lifetimes for these fatigue tests.

Results from creep tests conducted at 25 °C, 75 °C, and 125 °C showed that dispersion strengthened alloys had the greatest creep resistances. The dominant mechanism for these compositions was determined, by evaluating the creep exponents and activation energies, to be dislocation creep. The 63 Sn-37 Pb alloys gave results which corresponded to damage by grain boundary sliding. In addition, the offset after creep of gridlines initially engraved on the specimen surface supported the failure of the bulk eutectic solders by grain boundary sliding. The solid solution strengthened alloys, which resulted in the lowest creep resistance, were determined to fail by dislocation creep. Table 2-1 summarizes the data from these creep tests.

Table 2-1. Summary of creep results of bulk samples

Solder alloy	n, stress exponent	Qc, activation energy for creep
63 Sn-37 Pb	3.2	12.5 kcal/mol
AMT 63 Sn-37 Pb	2.8	-
HPM 63 Sn-37 Pb	3.5	12.1 kcal/mol
HPM Sn-Pb-2.5 In	4.2	-
HPM Sn-Pb-2.5 Cu	10.0	-
HPM Sn-Pb-5.0 Cu	8.8	29.6 kcal/mol
HPM Sn-Pb-2.5 Ni	13.2	-
HPM Sn-Pb-5.0 Ni	5.5	25.0 kcal/mol

Kuo proposed that the main failure mechanism of rapidly solidified Sn-Pb based alloys under creep-fatigue is cavity nucleation and growth [17]. In the case of eutectic solders, this would manifest as grain boundary cavitation. In the case of solid solution alloys, cavity formation may be due to cavitations from strain mismatches at triple junctions. In dispersion strengthened compositions cavity nucleation was attributed to the presence of dispersoids.

Physical Properties of Solder Joints

When a near eutectic Sn-Pb solder is allowed to reflow on a copper surface, a layer of intermetallics always forms between the copper and the eutectic solder, as shown in Figure 2-2. Initially the Cu is coated by a thin layer of the ε intermetallic phase, which consists of Cu_3Sn. Next a layer of the η phase, Cu_6Sn_5, grows in between the ε phase and the eutectic solder. Both intermetallic phases can grow considerably with time, even at room temperature [19].
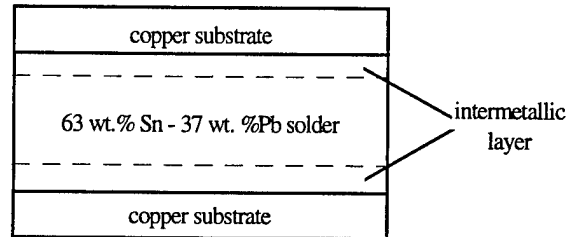
Figure 2-2. Side view of layers in a solder joint

The intermetallics are extremely brittle in comparison to the eutectic solder. This can lead to facile cleavage of intermetallic grains under stress. A large difference in the elastic moduli exists between the solder and the intermetallic layers, which can cause stress concentrations to form at the solder-intermetallic interface. Therefore this boundary may supply favored sites for crack initiation and propagation. Several studies have concluded that thicker intermetallic layers may decrease yield strengths [6,16, 20].

The effect of varying the concentrations of Sn and Pb on the mechanical properties of solder joints has been studied by a number of investigators. Because Pb has a higher melting point than Sn (327.4 °C compared to 231.9 °C), it is often used to raise the melting temperature of solder alloys. However, the shear strength of solders decreases with larger weight percentages of Pb. In addition, thermal fatigue lifetimes have been reported to decrease with increased amounts of Pb [11, 21]. Some of the properties of pure tin and pure lead are listed in Table 2-3. The elastic moduli for the intermetallic compounds was reported as 85.5 GPa and 108 GPa, for Cu_6Sn_5 and Cu_3Sn respectively [15].

The bulk and joint solder configurations contain differences which may lead to significantly different results for similar tests. As mentioned previously, solder joints contain a layer of intermetallics which is not found in bulk samples. The bulk solders tested previously at Washington University were tested in tension, while joints were tested in shear. Solder in joints is constrained at substrate interfaces not present in bulk samples. In solder joints, unlike bulk samples, the stress and strain distributions are not uniform, due to stress concentrations and variations of the cross-sectional area, due to fillets and imperfections. These differences lead to difficulties in directly comparing results from bulk tests to joint tests [22].

Table 2-2. Physical properties of pure Sn and Pb and 63Sn-37Pb solder [18, 23]

	Tin	Lead	63 Sn-37 Pb
Elastic modulus	44.9 GPa (20 °C)	16.1 GPa (20 °C)	30.6 GPa (20 °C)
Coefficient	23.5×10^{-6} 1/K (20°C)	29.0×10^{-6} 1/K (20°C)	25.0×10^{-6} 1/K (20°C)
of thermal	23.8×10^{-6} 1/K (100°C)	29.1×10^{-6} 1/K (100°C)	
expansion	24.2×10^{-6} 1/K (200°C)	30.0×10^{-6} 1/K (200°C)	
Melting point	231.93 °C	327.42 °C	183 °C
Tensile strength	14.5 MPa (20 °C)	16.8 MPa (20 °C)	
	11.0 MPa (100 °C)	12.1 MPa (60 °C)	
		4.5 MPa (200 °C)	
Density	7.3 g/cm^3 (20 °C)	11.35 g/cm^3 (20 °C)	8.34 g/cm^3 (20 °C)

Previous research on the mechanical properties of lap shear solder joints was conducted at Washington University by Baynham [24]. He used rapidly solidified powders with diameters ranging from 25 μm to 45 μm hand mixed with a commercial flux, Kester Sp244, to make solder pastes.

Shear tests were performed at room temperature at a constant crosshead speed of 1 x 10^{-3} in s^{-1}. Results showed that strengthening either by solid solution or by dispersion mechanisms of the 63 wt. % Sn-37 wt.% Pb increased the ultimate shear strength and decreased the ductility of the joint. 63 Sn-32 Pb-5 Ni gave significantly lower ductilities than any of the alloys tested. 95 Sn-5 Sb (maximum load of 323 lbs) resulted in one of the largest ultimate shear strengths of the samples tested, while 43 Sn- 57 Bi gave the lowest.

Solder joints were aged at 100 °C for 1 week and then tested in shear at room temperature. Results showed that the aged samples had ultimate shear strengths about 15% to 20% lower than the unaged samples. This weakening of the solder was attributed to the growth of the intermetallic layer thickness, by 20% to 40%, during aging. However, no analysis was done on the changes of the solder's microstructure after aging.

Low cycle fatigue tests were conducted at room temperature at displacement amplitudes of ± 2 mils, ± 1.5 mils, and ±1 mil. The displacement rate was kept constant at 1 x 10^{-3} in s^{-1} for all of the tests. Figure 2-3 shows the resulting lifetimes for all of the compositions tested. At a displacement amplitude of ± 1 mil, 63 Sn-32 Pb-5 Ni had the longest lifetime, followed by 63 Sn-34.5 Pb-2.5 Sb, 95 Sn-5 Sb, and then the remaining solid solution and dispersion strengthened alloys. The Sn-Pb and Sn-Bi eutectics gave the lowest lifetimes at this amplitude. 95 Sn-5 Sb exhibited some of the longest lifetimes at each displacement amplitude. 63 Sn-37 Pb displayed the longest lifetimes at greater

displacements, but the lowest lifetimes at small displacements. 43 Sn-57 Bi consistently had the lowest lifetimes of the samples tested.

Stress jump creep tests were conducted at 75 °C. 95 Sb-5 Sb displayed the best creep resistance, followed by the dispersion and solid solution strengthened alloys, and then the Sn-Pb eutectics. 43 Sn-37 Bi gave the lowest creep resistance of the alloys tested. It was postulated that 63 Sn-32 Pb-5 Ni had a high threshold stress associated with it, due to the difficulties experienced in conducting creep tests with this alloy. Table 2-4 summarizes these creep results and lists the deformation mechanisms proposed by Baynham. Because these tests were conducted at only one temperature, activation energies were not calculated. These values are needed to better differentiate between the possible deformation mechanisms.
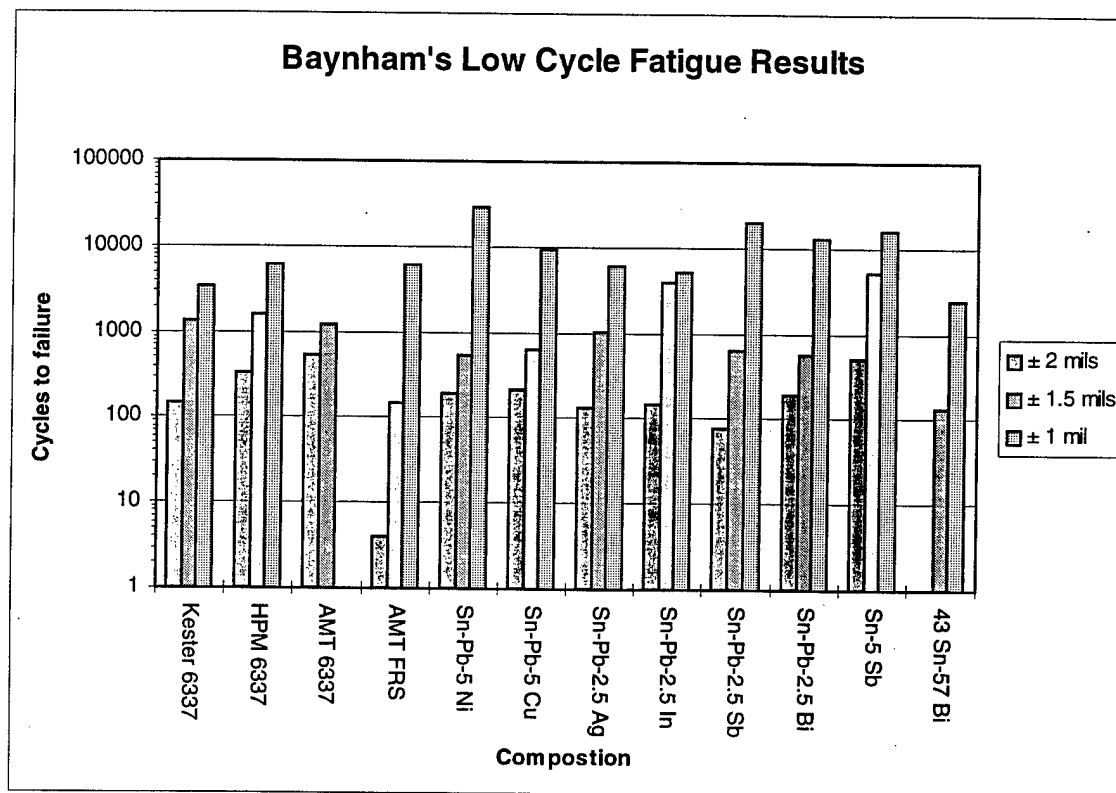
Figure 2-3. Room temperature low cycle fatigue test results of solder joints [24]

Table 2-3. Summary of creep results of lap shear joints

Composition	Composition Type	Creep Exponent	Proposed deformation mechanism
43 Sn-57 Bi	lead free	1.4	grain boundary sliding or diffusional creep
HPM 63 Sn-37 Pb	eutectic	3.4	dislocation creep
commercial 63 Sn-37 Pb	eutectic	3.7	dislocation creep
63 Sn-32.5 Pb-2.5 In	solid solution strengthened	8.9	dislocation glide
63 Sn-34.5 Pb-2.5 Bi	solid solution strengthened	2.5	grain boundary sliding or diffusional creep
63 Sn-34.5 Pb- 2.5 Sb	solid solution strengthened	5.0	dislocation glide
63 Sn-34.5 Pb-2.5 Ag	solid solution strengthened	6.0	dislocation glide
63 Sn-32 Pb-5 Cu	dispersion strengthened	3.7	dislocation creep
95 Sn-5 Sb	lead free	13.0	dislocation glide

Review of Thermomechanical Fatigue

Sn-Pb eutectic solder at room temperature is at 64% of its melting temperature expressed in degrees Kelvin (also called the homologous temperature, T_H). At 100 °C this solder is at 0.82 T_H. Thus, this material is subjected to damage from time and temperature dependent mechanisms such as creep, grain growth, and recrystallization, as well as athermal effects. Evaluating the deformation of solder during thermomechanical fatigue can become complicated as more than one mechanism may become dominant during different phases of the fatigue cycle [5].

Thermomechanical fatigue has been shown to affect a variety of materials. One example of this type of fatigue is found in metal matrix composites (MMC's), which are fabricated by placing reinforcing fibers in a metal matrix. These fibers usually have a considerably lower coefficient of thermal expansion than the metal matrix. An example of a MMC is SCS-6 / Ti-15-3, where the silicon carbide has a coefficient of thermal expansion of 9.0 x 10^{-6} °C^{-1} compared to titanium's coefficient of 4.9 x 10^{-6} °C^{-1}. Whenever a metal matrix composite is heated or cooled, internal stresses and strains are produced from the different expansion rates of the two materials. Large temperature ranges can therefore be damaging to this type of materials [25].

Research has been conducted on the thermomechanical fatigue of steels in the severe conditions of gas turbine blades and nuclear reactor power plant pipes. However, much of this work can not be easily applied to the fatigue of solder because of the significantly lower relative temperature ranges considered. The 304 stainless steel used in nuclear plants, for example, was researched at homologous temperatures of 0.2 to 0.6 (from 25 °C to 650 °C). At these temperatures, the microstructures of the materials do not significantly change during testing, and creep and other time dependent mechanisms become dominant for only a small portion of the test. No simple prediction method was

found to apply to the thermomechanical fatigue of 304 stainless steel, even though it may be a less complex phenomena than the fatigue of solder, [26].

One possible damage mechanism for the thermomechanical fatigue of solder is from low temperature, isothermal, low-cycle (strain controlled) fatigue. Generally, at low temperatures (less than 0.5 T_H) damage in materials from low cycle fatigue is caused by the initiation and propagation of microcracks. As the testing temperature is increased, the mode of failure changes from transgranular crack propagation to the intergranular nucleation of cracks at grain boundary triple points or at cavities within the grain boundary. Fatigue lifetimes are usually found to decrease with increased temperatures. In addition, fatigue lives increase with finer grain sizes because grain boundaries provide obstacles to the propagation of fatigue cracks [14].

The low cycle fatigue life of a metal is generally described by the Coffin-Mason relationship:

$$\Delta\varepsilon_p/2 = \varepsilon'_f (2N_f)^c \qquad (2\text{-}3)$$

where $\Delta\varepsilon_p/2$ is the plastic strain amplitude, N_f is the number of cycles to failure, ε'_f is the fatigue ductility coefficient, and c is the fatigue ductility coefficient. The area in a hysteresis curve in a stress versus strain plot can be used as a measure of the energy dissipated for each cycle, which represents the amount of work done to plastically deform the material. Thus a wider hysteresis loop indicates that larger amounts of plastic strain are being applied. Samples with wider loops will have lower fatigue lives than samples which experience less plastic strain, as evidenced by their thinner hysteresis loops [27].

Creep damage mechanisms can become dominant if the testing temperature is greater than 0.5 T_H. A general equation for the steady state creep rate is given below:

$$\dot{\varepsilon}_{ss} = A\sigma^n e^{-Q_c/RT} \qquad (2\text{-}4)$$

where A is a material constant, Q_c is the creep activation energy, R is the universal gas constant, and T is the temperature expressed in Kelvin.

Depending on the temperature, stress, and material characteristics, different types of creep mechanisms can dominate. These include vacancy diffusion (Nabarro-Herring), grain boundary diffusion (Coble), and dislocation climb and glide creep. Coble and Nabarro-Herring creep are proportional to $1/d^3$ and $1/d^2$, respectively, where d is the material's grain size. Damage during creep can emerge as creep cracks, void nucleation and growth, and microstructural changes [5,28].

Microstructural changes during thermomechanical fatigue can significantly alter the material's mechanical properties. The release of strain energy can occur by the recrystallization and growth of strain-free grains. This usually results in a softer, weaker material with greater ductilities. The rate at which a material recrystallizes increases with strain and temperature, and is given by

$$\tau = Ae^{-Q_r/RT} \quad (2\text{-}5)$$

where $1/\tau$ is the rate at which 50% of the material recrystallizes, Q_r is the activation energy, R is the gas constant, and T is the temperature expressed in Kelvin.

Grains can grow at substantial rates even at room temperature in eutectic Sn-Pb solders. The rate of grain growth is also increased with strain and temperature. The grain size D after some time t can be given by

$$D^2 = D_o^2 + kte^{-Q/RT} \quad (2\text{-}6)$$

where D_o is the initial grain size, k is a constant, t is time, and Q, R, and T are the same as defined above [29].

The relation of the yield stress of a material to its grain size as is usually described by the Hall-Petch relationship:

$$\sigma_y = \sigma_o + k\, d^{-1/2} \quad (2\text{-}7)$$

where σ_y is the yield strength, k is a constant, and d is the grain size. This equation implies that the yield stress should increase as the grain size is decreased [28]. Conversely, at high homologous temperatures, flow stress increases with increasing grain size due to the increase in thermally activated mechanisms such as grain boundary sliding [30].

Table 2-5 summarizes the relationships of the damage mechanisms mentioned above to grain size. Lower temperature damage mechanisms generally decrease with smaller grain sizes, while high temperature (T>0.5T_H) mechanisms decrease with larger grains.

Table 2-4. Relationships between grain size and various deformation mechanisms

test type	grain size dependence
low cycle fatigue	longer lives with decreased d
creep	Coble: creep rate $\alpha\, 1/d^3$
	Nabarro-Herring: creep rate $\alpha\, 1/d^2$
	other creep mechanisms: no dependence on d
flow stress	low temperatures: $\sigma_y \alpha\, d^{-1/2}$
	high temperatures: $\sigma_y \alpha\, d$

A unique damage mechanism has been reported by Grivas, Morris, and Frear in high temperature tests of near eutectic Sn-Pb solder joints. They observed the development of coarsened bands of both Sn-rich and Pb-rich phases in the solder developing parallel to

the Cu-solder interface in samples subjected to loading in shear. In addition, Morris and Wei observed a preferential coarsening of Sn-rich grains. Cracks were observed to propagate through this coarsened band. A drawing of the microstructure of the heterogeneous coarsened band is included in Figure 2-4. This type of damage mechanism has been reported for initially lamellar eutectic solder joints for a variety of thermal and loading conditions, including creep, thermal shock, slow thermal fatigue, creep, and thermomechanical fatigue.
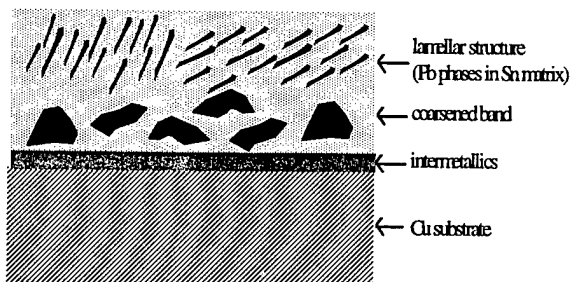
Figure 2-4. Schematic of coarsened band in Sn-Pb eutectic solder

The development of coarsened bands in fatigued solder has been explained by the stress concentrations that are expected to exist near the solder-intermetallic interface due to the large difference in elastic moduli. The stressed solder material, especially along soft colony boundaries, will recrystallize into fine, globular grains which will quickly grow. Shear deformation will concentrate in the relatively soft recrystallized materials, which locally increases the rate of the coarsening process. The soft, coarsened area will act like a narrow crack and spread through the solder in the direction of the applied shear. Small interfacial cracks form in the coarsened regions by cavity growth and interlinkage. These cracks then propagate through the coarsened region until the joints fail [6, 8,11,31,32].

Research has been performed on the effects of varying the test parameters (such as frequencies, deformation rates, and hold times) of thermomechanical fatigue tests. Increasing the frequency of tests has been observed to increase the solder lifetimes, due to the decreased times spent at higher temperatures. Increased frequencies decreases the time for temperature dependent mechanisms such as creep and grain growth to occur. [33].

Deformation mechanisms have been observed to change as the deformation rates of thermomechanical fatigue tests are changed. Strain rates during thermomechanical fatigue of less than 2.8×10^{-4} sec^{-1} have been shown to result in similar microstructural changes as solder joints in service conditions. Strain is accommodated in eutectic colony boundaries, which are observed to heterogeneosly coarsen. Intergranular cracks then develop through the coarsened Sn-rich phases. Strain rates faster than 5.6×10^{-4} sec^{-1} cause strain concentrations to develop as the grains are not able to slide and rotate rapidly enough to accommodate imposed strains. These faster strain rates can lead to heterogeneous coarsening in thin regions of the solder [34,35].

Hold times were observed to have different effects at the two extremes of a temperature cycle. Hold times at low temperatures (at or below room temperature) were determined to have little effect on the thermomechanical fatigue of solders. This was attributed to time dependent damage mechanisms in solder at low temperatures having less significance than athermal damage mechanisms. However, at elevated temperatures hold times greatly affected fatigue results. With no hold times the solder was observed to homogeneously coarsen instead of forming coarsened bands. Fatigued samples with hold times displayed heterogeneous grain growth at cell boundaries and a relaxation of load to zero pounds in a short time. Shorter hold times in cyclic creep tests resulted in much longer lifetimes, as damage accumulation from creep was significantly decreased.

Changing the temperature extremes of thermomechanical tests was shown to drastically change the operating damage mechanisms. The rates of high temperature mechanisms such as creep, grain growth, and recrystallization all depend on the temperature. Therefore, to accurately model service conditions, the temperature range for thermomechanical fatigue tests should be kept close to the temperatures experienced in actual electronic parts [5,34].

A few metallurgical techniques have been proposed to increase the lifetimes of thermomechanically fatigued, near eutectic Sn-Pb solder joints. One suggested method is to alter processing techniques to produce a fine-grained, equiaxed, superplastic microstructure. However, as mentioned previously, it is difficult to create and retain this structure for the needed lifetime of electronic solder joints.

Two other proposed methods involve the addition of particles to the Sn-Pb near eutectic matrix. One of these techniques would use these third phase particles to homogenize the material by inhibiting the creation of the lamellar microstructure in favor of a equiaxed microstructure. This would hopefully reduce the formation of heterogeneously coarsened bands by eliminating strain concentrations in the solder. Examples of this method include the additions of In and Cd to 60 Sn-40 Pb solders, which have been shown to create a more uniform and degenerate, and less eutectic, microstructure.

The addition of dispersoid particles to Sn-Pb has also been suggested to increase the fatigue resistance of solder joints. These particles would strengthen the solder matrix by creating obstacles in the solder to the growth of recrystallized and coarsened bands [6,8,11].

A limited amount of data is available on results from thermomechanical fatigue tests, due to a majority of tests being conducted on actual components where strains and stresses could not be measured. The effect of Ag additions to eutectic Sn-Pb solder has been examined by a few researchers, with little agreement between authors if the Ag results in longer lifetimes than eutectic solders. Work by Jarboe indicates that 42Sn-58Bi, 62Sn-36Pb-2Ag, 63Sn-37Pb, and 59.5Sn-37.4Pb-3.1Sb all have comparable lifetimes, and that 95Sn-5Sb has about three times the lifetime of the other alloys. A possible correlation between greater strength solders and fatigue resistance was observed by a few authors.

No standard testing methodology currently exists for the thermomechanical fatigue of solder [8].

Several authors have tried to apply standard lifetime predictive models to the thermomechanical fatigue of solders. These models includes Coffin-Manson, strain-life relationships, creep-fatigue life, damage integrals, and strain-range partitioning models. However, all of these prediction techniques assume that microstructural changes during the test will not significantly affect results. In solder joints effects such as recrystallization and grain growth have been shown to play a significant role in the failure of the samples. The predictive models employed could not account for these changes, and thus were unable to accurately predict fatigue lifetimes [36, 37, 38].

3. RESEARCH OBJECTIVES AND APPROACH

The objectives of the research program are to: (i) determine the effects of microstructural variables, test temperature, stress/strain amplitude, and frequency on the thermomechanical fatigue behavior of in-situ composite solders, and (ii) develop guidelines for producing fatigue resistant microstructures of Sn-Pb solder.

The specific goals of the current research are to use thermomechanical fatigue tests to simulate usage conditions for solder joints used in SMT configurations. These tests were conducted on in-situ lap shear joints so that mechanical properties, as well as lifetimes, could be evaluated. The objectives are to rank the performance of several different compositions under TMF conditions, while at the same time gaining a better understanding of which damage mechanisms dominate for the different types of solder compositions.

Solder Compositions Examined

The compositions of the solders under examination are shown in Table 3-1. The microstructural classifications were selected based on previous work by Kuo [17]. The eutectic solders manufactured by IEM Fusion, Inc. and Advanced Metals Technology, Inc. of Branford, Connecticut are commercial grade 6337 pastes. The FRS (fatigue resistant solder) was designed by AMT and Hughes Aircraft to produce a more uniform, fine grain solder than 6337, and consists of a base eutectic Sn-Pb solder with small amounts of added strengthening elements [32].

The solders contributed by High Performance Materials (HPM) of St. Louis, MO were manufactured using a rapid solidification process which involved a combination of induction melting and gas atomization to produce fine, spherical solder powders. This process produced the small particle sizes needed to produce the fine dispersoids required for effective dispersion strengthening [30]. The powders were sieved to powder diameters between 25 and 45 µm. Pastes were made with these powder by IEM using an IEM flux. The pastes for the shear tests of HPM solder powders were made at Washington University, by mixing by hand the powders with Kester SP 244 flux (supplied by the Kester Solder Company).

Table 3-1. Solder compositions under examination

Composition	Company	Melting Temp. °C	Microstructure Type
63Sn-37Pb	HPM	191	eutectic
63Sn-37Pb	IEM	191	eutectic
63Sn-37Pb	AMT	191	eutectic
FRS	AMT	191	modified eutectic
63Sn-34.5Pb-2.5Ni	HPM	190	dispersion strengthened
63Sn-32Pb-5Ni	HPM	190	dispersion strengthened
63Sn-32Pb-5Cu	HPM	190	dispersion strengthened
63Sn-34.5Pb-2.5In	HPM	189	solid solution strengthened
63Sn-34.5Pb-2.5Ag	HPM	191	solid solution strengthened
63Sn-34.5Pb-2.5Bi	HPM	189	solid solution strengthened
63Sn-34.5Pb-2.5Sb	HPM	193	solid solution strengthened
95Sn-5Sb	HPM	240	lead free
90Sn-3.2Ag-6.8Bi	IEM	220	lead free
86Sn-3Ag-4.2Bi-6.8In	IEM	211	lead free
42Sn-58Bi	HPM	158	lead free

Table 3-2 shows that nickel and copper have an almost negligible solubility in either Sn or Pb alloys [9]. Ni and Cu will therefore tend to form intermetallic compounds, such as Cu_6Sn_5 and Ni_3Sn_4, when added to a Sn-Pb solder. Nickel has been shown to be more effective than copper in forming a large volume fraction of fine dispersoids, and should therefore be more effective in improving the tensile strength and other mechanical properties of the solder, according to equation 2-2. Indium, bismuth, silver, and antimony all have relatively high solid solubilities in Sn-rich and Pb-rich phases. Therefore, the Sn-Pb-In, Sn-Pb-Bi, Sn-Pb-Ag, and Sn-Pb-Sb compositions tested in this research tended to form solid solutions [17].

Table 3-2. Solid solubility of ternary alloying elements in Sn-rich and Pb-rich phases

Solder alloy	Ternary phase	Solid solubility at 150°C in Sn	Solid solubility at 150 °C in Pb	Melting point of the ternary element
Sn-Pb-In	-	4 wt%	70 wt%	In: 157°C
Sn-Pb-Bi	-	10 wt%	20 wt%	Bi: 271 °C
Sn-Pb-Sb	SbSn	4 wt%	3.5 wt%	Sb: 631 °C
Sn-Pb-Ag	Ag_3Sn	0.05 wt%	0.05 wt%	Ag: 962 °C
Sn-Pb-Cu	Cu_6Sn_5	<<0.05 wt%	<<0.05 wt%	Cu: 1085 °C
Sn-Pb-Ni	Ni_3Sn_4	<<0.05 wt%	<<0.05 wt%	Ni: 1453 °C

Overview of Tests Conducted

Shear tests of lap shear solder joints were conducted at a displacement rate of 1.67×10^{-6} in/sec on a MTS hydraulic test frame, at temperatures of 20 °C, 75 °C, and 125 °C. The maximum loads, extensions at maximum loads, yield strengths, extensions at yield strength, elastic modulus, extensions at 50% load drops, and areas under the load vs. extension curve were all determined.

Isothermal low cycle fatigue tests were conducted at 75 °C and 125 °C at a constant displacement rate of 1×10^{-3} in/sec and a displacement amplitude of ± 1 mil. An MTS hydraulic test frame was used for all of these tests.

Creep properties were determined at 20 °C, 75 C°, and 125 C°, using stress jump tests. Stress exponents were calculated at each temperature by plotting the applied stress versus the steady state creep rate for constant temperatures on a log-log plot and using a power law regression. Activation energies were determined by fitting a line to a plot of the natural logarithm of the steady state strain rate versus the reciprocal of temperature (in units of Kelvin) for a constant applied stress.

Thermomechanical fatigue tests were conducted by applying in phase, triangular temperature (25 °C to 100 °C) and extension (± 0.7 mils) waveforms. Hysteresis plots of load versus extension were recorded for every other cycle. These plots were analyzed to measure the number of cycles to failure (defined as a 50% load drop from the maximum load in the initial cycle). In addition, plots were made for each test of the area under each hysteresis curve and the maximum cyclic load versus the number of cycles. Table 3-3 shows which of the tests was conducted for each solder composition. Table 3-4 lists the conditions under which lap shear joints were processed for the different tests in this research.

Table 3-3. Test Matrix

Composition	Shear	High temperature low cycle fatigue	Creep	TMF
HPM 63Sn-37Pb	x	x	x	x
IEM 63Sn-37Pb	x			x
AMT 63Sn-37Pb	x	x	x	x
AMT FRS	x			x
HPM 63Sn-34.5Pb-2.5Ni	x			x
HPM 63Sn-32Pb-5Ni	x	x	x	x
HPM 63Sn-32Pb-5Cu	x			x
HPM 63Sn-34.5Pb-2.5In	x	x	x	x
HPM 63Sn-34.5Pb-2.5Ag	x			x
HPM 63Sn-34.5Pb-2.5Bi	x			
HPM 63Sn-34.5Pb-2.5Sb	x			
HPM 95Sn-5Sb	x		x	x
HPM Sn-Ag-Bi	x			x
HPM Sn-Ag-Bi-In	x			x
HPM 42Sn-58Bi	x			

Table 3-4. Summary of joint processing parameters for various tests

test type	flux	paste mixing process	mechanical pump (low vacuum)	mechanical and diffusion pump (high vacuum)
Baynham's	Kester SP244	by hand at Washington University		x
Shear	Kester SP244	by hand at Washington University	x	
Creep, low cycle fatigue, thermomechanical fatigue	IEM	by IEM		x

4. RESULTS AND DISCUSSION

Initial Microstructure

The initial microstructures of the solder in the lap shear joints were determined from micrographs. An analysis using EDS showed that the white phases in the micrographs are Pb-rich phases and grey phases are Sn-rich. These micrographs were taken using polished (unetched) samples in a scanning electron microscope (SEM) operating in backscattered mode. This mode was not able to resolve the different phases for the non-Sn-Pb based alloys, such as Sn-5Sb and 90Sn-3.2Ag-6.8Bi. All of the Sn-Pb based compositions displayed a globular microstructure of Pb rich phases in a Sn matrix.

Table 4-1 lists the measurements made for the as-made samples. The error in measuring the grain sizes of Pb-rich phases was estimated as ±5%, and the error in measuring the volume % of Pb phases was estimated as ±10%. The two solder alloys containing Ni dispersoids showed significantly thicker intermetallic layers and lower volume percentages of Pb-rich phases. The eutectic 63Sn-37Pb had the largest average Pb grain sizes of the alloys tested. This suggests that the addition of ternary particles to eutectic solder impedes grain growth during solidification and cooling after reflow.

Table 4-1. Analysis of as-made samples

Composition	Intermetallic thickness (μm)	Average Pb-rich grain diameter (μm)	Volume % Pb-rich phases
HPM 63Sn-37Pb	2.5	0.86	20.2%
AMT 63Sn-37Pb	2.4	0.97	18.0%
IEM 63Sn-37Pb	1.6	0.95	21.1%
AMT FRS	3.1	1.00	25.7%
63Sn-34.5Pb-2.5Ni	24.0	0.53	10.7%
63Sn-32Pb-5Ni	16.4	0.74	14.1%
63Sn-32Pb-5Cu	3.5	0.76	18.5%
63Sn-34.5Pb-2.5Ag	4.0	0.70	23.9%
63Sn-34.5Pb-2.5In	2.9	0.84	21.4%
90Sn-3.2Ag-6.8Bi	7.2		

Table 4-2 gives the results of an EDS analysis of the microstructural phases in the as-made samples. This data indicates that initially the Pb-rich phases contain from 25 wt. % to 55 wt. % of Sn, while Sn-rich phases contain at the most 20 wt.% of Pb. The Sn-rich phases are close to pure Sn, while the Pb-rich phases contain significant concentrations of Sn.

Table 4-2. EDS analysis of as-made solder joints

composition	element X	Pb-rich phase			Sn-rich phase		
		wt.% Sn	wt.% Pb	wt.% X	wt.% Sn	wt.% Pb	wt.% X
AMT 6337	-	42.8 %	56.8 %	-	85.3 %	14.6 %	-
IEM 6337	-	34.4 %	65.7 %	-	85.9 %	13.7 %	-
AMT FRS	-	40.8 %	57.5 %	-	96.2 %	35.1 %	-
Sn-Pb-2.5Ni	Ni	44.0 %	54.3 %	0.9 %	91.1 %	6.1 %	1.9 %
Sn-Pb-5Ni	Ni	26.6 %	71.7 %	1.3 %	91.4 %	0.0 %	6.5 %
Sn-Pb-5Cu	Cu	48.4 %	51.4 %	0.3 %	98.2 %	1.6 %	0.2 %
Sn-Pb-2.5Ag	Ag	54.4 %	42.4 %	2.9 %	84.4 %	14.6 %	0.4 %
Sn-Pb-2.5In	In	26.3 %	72.1 %	0.0 %	80.8 %	18.7 %	0.2 %

Shear Tests

The maximum loads and extensions at maximum load for shear tests conducted at a constant displacement rate of 1.67×10^{-6} in/sec are included in Table 4-3. Results from the shear tests show that the ultimate shear strength of the solder joints decreased rapidly as the testing temperature was increased. The maximum loads at room temperature were much lower than those reported by Baynham, due to the lower displacement rates employed in this research.

The compositions with higher melting points displayed better results than the other alloys. The Sn-Ag-Bi and Sn-Ag-Bi-In compositions had significantly larger ultimate strengths and larger extensions at maximum load at all three temperatures. Sn-5Sb gave extensions at maximum load that were greater at each temperature than the other compositions.

The dispersion strengthened Sn-Pb-5 Ni showed a higher than average shear strength at room temperature, but only average strengths at elevated temperatures. Sn-Bi had the greatest ductilities at room temperature among the alloys tested, but had the lowest maximum loads.

Table 4-3. Results from shear tests

Composition	25 °C		75 °C		125 °C	
	Max load (lbs)	Extension at Max load (mils)	Max load (lbs)	Extension at Max load (mils)	Max load (lbs)	Extension at max load (mils)
AMT 6337	155	2.4	76	1.5	49	1.0
AMT-FRS	165	2.0	96	1.3	40	0.9
HPM 6337	135	2.0	119	1.9	33	0.7
Sn-Pb-5Ni	221	3.1	108	1.6	44	0.7
Sn-Pb-2.5Ni	138	2.5	110	1.7	67	1.0
Sn-Pb-5Cu	172	2.7	120	1.9	43	1.0
Sn-Pb-2.5In	156	2.5	100	1.3	34	0.6
Sn-Pb-2.5Ag	167	2.8	140	1.7	45	0.6
Sn-Pb-2.5Bi	142	2.1	103	1.6	39	0.8
Sn-Pb-2.5Sb	154	2.1	101	1.5	43	0.6
Sn-5Sb	169	5.0	126	3.3	66	1.1
Sn-Ag-Bi	292	4.9	244	2.8	52	0.9
Sn-Ag-Bi-In	332	5.1	203	2.9	66	1.4
42Sn-58Bi	121	17.9	122	1.7	27	0.7

Micrographs of the fracture surface reveal many voids in the failed samples, with visible void sizes ranging from 2 to 40 mils in diameter. Sn-Pb-5Ni and Sn-Pb-5Cu, two of the dispersion strengthened alloys, contained the largest number of voids. A large amount of voids in a sample will result in a large decrease in the cross sectional area, and thus increase the shear stress on the solder joint. Due to the presence of large voids, the results from the shear tests contain large inaccuracies and are only used as general measures of the relative strengths of the solder joints.

Two HPM 63Sn-37Pb lap shear solder joints were tested in shear, one at room temperature and one at 125 °C, until the load had dropped by 50% from the maximum value. The tests were then stopped and each joint was polished for SEM examination. SEM analysis of the shear sample tested at room temperature indicates that the joint fails by interlinkage of small voids throughout the solder. There was no evidence of cracks forming near the Cu-solder interface.

Analysis of shear samples tested at 125 °C showed that cracks formed in the solder near the Cu substrate. An EDS analysis near this crack indicates that the solder immediately above the crack contains 28.8 wt.% Cu, while directly below the crack the solder contains

7.0 wt.% Cu. The EDS work suggests that the crack propagates in the interface between the solder and the intermetallic layer.

A possible explanation for how the cracks develop in the lap shear solder joint is derived from the differences in the elastic moduli of the solder and intermetallics, especially at elevated temperatures. Sn-Pb eutectic solder is expected to soften significantly as the temperature is changed from room temperature (0.64 T_H) to 125 °C (0.86 T_H). Conversely, intermetallics generally retain their strengths to very high temperatures. Therefore, it is probable that a larger difference in strengths of the solder and the intermetallics exists at higher temperatures. Research by Hutchinson has shown that an energy minimum exists a small distance away from the interface of 2 elastic materials, and that cracks are prone to initiate at the energy minimum [15]. Thus the difference in elastic moduli at elevated temperature would cause the solder-intermetallics interface to be a favored site for the initiation of cracks.

Effect of Vacuum on Void Formation

The solder joints used for the shear tests were manufactured using low vacuum. The fracture surfaces of these joints contained many large voids. Lap shear joints were also made using the same solder paste with a high vacuum, and were tested with shear tests at room temperature. Very few voids were visible under a stereomicroscope for the samples made in a high vacuum. It was concluded that the use of a higher vacuum during joint processing yields lower amounts of internal voids. The diffusion pump was used in the manufacturing of the remainder of the solder joints used in this research.

Microhardness Results

Microhardness tests were conducted for a few selected compositions at room temperature. The results from these tests are included as Table 4-4. The alloys with the largest microhardness values, Sn-5Sb and Sn-Pb-5Ni, also had the largest ultimate shear strengths at room temperature.

Table 4-4. Microhardness results

composition	average hardness	standard deviation
HPM 63Sn-37Pb	13.3 VHN	± 1.2 VHN
AMT 63Sn-37Pb	13.2 VHN	± 1.5 VHN
Sn-Pb-5Ni	19.8 VHN	± 2.1 VHN
Sn-5Sb	23.0 VHN	± 2.2 VHN
Sn-Pb-2.5In	16.5 VHN	± 2.7 VHN
Copper substrate	126.8 VHN	± 19.6 VHN

Effect of Aging on the Solder Microstructure

A lap shear solder joint of HPM 63Sn-37Pb was aged for 12 hours at 100 °C. The measurements made for this aged sample are in Table 4-5. Aging the sample resulted in significant growth and a larger volume percentage of the Pb-rich grains. The intermetallic layer was not observed to grow during this aging process.

Table 4-5. Analysis of aged HPM 63Sn-37Pb sample

	as-made sample	aged sample	% difference
average Pb-rich grain diameter	0.86 μm	2.40 μm	179 %
intermetallic thickness	2.50 μm	2.48 μm	-0.8 %
volume % Pb-rich phases	20.2%	43%	113 %

Creep Tests

Jump creep tests were conducted at room temperature, 75 °C, and 125 °C. Table 4-6 contains creep exponents and activation energies calculated from the creep data.

Sn-Pb-5 Ni seemed to have a threshold stress below which the solder joint would not creep (around 150 lbs at room temperature, 75 lbs at 75 °C, and 15 lbs at 125 °C). The presence of a threshold stress made it difficult to obtain accurate creep data for this solder. The final row in Table 4-6 contains calculations for creep exponents for this alloy with the threshold stress subtracted from the applied stresses. At all three testing temperatures Sn-Pb-5Ni (a dispersion strengthened alloy) and Sn-5Sb (an alloy with a high melting temperature) displayed higher creep resistances then Sn-Pb-2.5In (solid solution strengthened), AMT 63Sn-37Pb (eutectic), and HPM 63Sn-37Pb (eutectic).

Table 4-6. Calculated creep exponents and activation energies

composition	creep exponent			activation energy (Kcal/mol)
	room temperature	75 °C	125 °C	
HPM 63Sn-37Pb	10.0	3.98	3.33	30.8
AMT 63Sn-37Pb	9.3	4.88	3.07	30.4
Sn-Pb-2.5In	10.5	5.12	4.41	34.2
Sn-5Sb	5.12	33.8	9.48	
Sn-Pb-5Ni	14.7	21.8	21.8	177.3
Sn-Pb-5Ni (threshold stress subtracted)		2.41	4.19	11.3

The activation energies calculated for both eutectic Sn-Pb alloys and for Sn-Pb-2.5 In are close to the activation energy in Sn and Pb for lattice self-diffusion. Creep activation energies were calculated using the results from 75 °C and 125 °C, which had similar creep exponents. The creep exponents and activation energies for all three of these compositions are in the range for dislocation climb. The large difference in creep exponents at room temperature as compared to the elevated temperature tests for these three alloys indicates that a different deformation mechanism dominates at room temperature. Because only a few data points were obtained for Sn-Pb-5Ni it was not possible to accurately determine the dominant creep deformation mechanism. The activation energy was not determined for Sn-5Sb because the creep exponent varied widely at the different temperatures.

The results from the creep tests of lap shear solder joints differ from Kuo's results for bulk solder samples. Kuo found that bulk samples of 63Sn-37Pb failed by grain boundary sliding and had activation energies close to that for grain boundary self diffusion. The lap shear creep samples described above to deform by dislocation climb. The differences between the bulk and joint properties may be due to the Cu-solder interface constraining the solder in joints or because of the presence of an intermetallic layer in joint samples. Kuo's results gave similar results to tests of lap shear joints for the creep deformation mechanism of solid solution alloys and for the relative ranking of the solders compositions.

Creep tests of AMT and HPM 63Sn-37Pb at room temperature and 125 °C were conducted for three hours. The tests were then stopped and the samples were polished for SEM examination. A SEM examination of both Sn-Pb eutectic alloys tested at room temperature reveals no traces of cracks near the Cu-solder interface. There is some evidence that these joints deformed by the interlinkage of small voids by cracks throughout the solder joint. Both of the samples deformed at 125 °C contained cracks running parallel to the Cu substrate, possibly at the interface between the intermetallic layer and the solder or in the solder near the interface. These results are similar to the results obtained for 63Sn-37Pb deformed in shear, as described previously. The large difference in creep exponents determined for room temperature and elevated temperature creep tests supports a difference in damage mechanisms between these temperatures. This is evidenced by the difference in crack propagation sites in samples tested at room temperatures and at 125 °C.

Low Cycle Fatigue Tests

Low cycle (displacement controlled) fatigue tests were conducted at a frequency of 0.25 Hz and a displacement amplitude of ±1.0 mils for selected solder alloys at 75 °C and 125 °C. The results from these tests are listed in Table 4-7.

Sn-Pb-5Ni displayed the greatest fatigue resistance at all three temperatures. This is evidence that the dispersion strengthened alloys keep their strengthened properties at relatively high temperatures. At elevated temperatures, Sn-Pb-2.5 In had the lowest fatigue lifetime of the samples tested, which may be due to solid solution strengthening

23

losing its effectiveness at elevated temperatures. HPM 63Sn-37Pb showed greater fatigue resistances than AMT 63Sn-37Pb at all three temperatures.

Table 4-7. Low cycle fatigue data at elevated temperature

composition	temperature	maximum load, initial cycle (lbs)	cycles to failure
AMT 63Sn-37Pb	75 °C	116.0	1038
HPM 63Sn-37Pb	75 °C	108.9	3878
Sn-Pb-5 Ni	75 °C	125.8	3684
Sn-Pb-2.5 In	75 °C	108.9	464
AMT 63Sn-37Pb	125 °C	113.1	38
HPM 63Sn-37Pb	125 °C	79.8	578
Sn-Pb-5 Ni	125 °C	113.3	1116
Sn-Pb-2.5 In	125 °C	148.7	32

Effect of Altering the Paste Mixing Process

Literature shows that the viscosity of solder pastes has a large effect on the paste's reflow characteristics. Solder joints made with pastes with viscosities that are too low or too large may result in the formation of voids, blowholes, pinholes, and other defects. Solder paste has a thixotropic rheology, which means that the paste's viscosity decreases as it is subjected to a constant shear rate. Hence, the viscosity of a paste will change during mixing [42, 43].

An examination was made on the effects on thermomechanically fatigued tests by how solder powders and fluxes were mixed. Pastes made at Washington University were mixed by hand using no controls on the solders' viscosity. IEM mixed solder powders and fluxes while measuring viscosities to ensure proper paste qualities. All of the pastes which used Kester SP244 flux were mixed at Washington University.

Table 4-8 compares the results of using of solder pastes mixed by IEM and by Washington University on thermomechanical fatigue tests of HPM 63Sn-37Pb. Pastes mixed by IEM resulted in more than twice the lifetimes and greater than 15% increases in initial maximum loads than pastes mixed by hand. Therefore, all of the thermomechanical fatigue tests in this research were conducted using samples made with pastes mixed by IEM, which had superior results.

Table 4-8. Effect of paste mixing process on thermomechanical fatigue tests of HPM 63Sn-37Pb

flux used	paste manufacturer	thermomechanical fatigue tests	
		average cycles to failure	average maximum load in 1st cycle
Kester SP 244	Washington University, paste mixed by hand	53	80.3
IEM's flux	Washington University, paste mixed by hand	41	77.1
IEM's flux	IEM	116	93.1

Qualitative Examination of Wetting Characteristics

As discussed previously, it is important to have solders with good wetting and solderability characteristics to produce electronic parts with high quality solder joints. Sample SMT circuit boards were made by EMPF (Electronic Manufacturing Productivity Facility) and visually inspected. The results are listed in Table 4-9. The Sn-Pb eutectic solders yielded the best joints, while most of the alloys with ternary additions had joints with decreased wetting qualities.

Table 4-9. Visual inspection of SMT circuits made with different solder alloys

solder composition	visual observations of the solder joints
HPM 63Sn-37Pb	good wetting, solder balls, shiny joints, nice fillets
Commercial 63Sn-37Pb	good fillets, shiny, grainy appearance, did not wet entire pads, solder balls
Sn-Pb-5Cu	good wetting, solder balls, shiny joints, nice fillets
Sn-Pb-5Ni	rough and dull appearance, solder pooling, did not wet as well as HPM 63Sn-37Pb
Sn-Pb-2.5Ni	less roughness, some voids, pin holes, solder-balls, good wetting
Sn-Pb-2.5In	shiny appearance, solder balling, capillary flow-up
Sn-Pb-2.5Ag	grainy appearance, solder balling, pitting
Sn-Bi	good wetting, grainy, shiny, solder balling
Sn-Ag-Bi	good wetting, dull appearance, solder balls
Sn-Ag-Bi-In	mediocre wetting, dull appearance, solder balls, some dewetting
Sn-5Sb	shiny appearance, dewetting, solder balls, pooling on pads

Thermomechanical Fatigue Results

Thermomechanical fatigue results were obtained for 12 solder alloys using in-phase, triangular waveforms for temperature and displacement with ranges of 25 °C to 100 °C and -0.7 mils to 0.7 mils, respectively. Lifetimes (defined as the cycle in which the

maximum cyclic load had dropped by 50% from the initial cycle) and maximum loads during the initial cycle for these tests are listed in Table 4-10.

The 95Sn-5Sb alloy, the solder with the highest melting point (240 °C, compared to 190 °C for the near eutectic Sn-Pb alloys), resulted in the longest thermomechanical fatigue lifetimes. After 280 cycles both joints for this composition still had maximum cyclic loads around 80% of the maximum load during the initial cycle. Sn-Pb-5Ni, a dispersion strengthened alloy, had the second longest lifetime, followed by the other two dispersion strengthened alloys (Sn-Pb-2.5 Ni and Sn-Pb-5 Cu) and the other two high melting point alloys (Sn-Ag-Bi and Sn-Ag-Bi-In). The 63Sn-37Pb alloys, both from commercial sources and from HPM, ranked next in lifetimes. The two solid solution alloys that were tested, Sn-Pb-2.5 In and Sn-Pb-2.5 Ag, produced the worst lifetimes.

Five samples of AMT 63Sn-37Pb were tested to measure the consistencies of the thermomechanical fatigue tests. The standard deviation for the number of cycles to failure was measured as 33.3, while the standard deviation for the maximum load during the first cycle was 7.8. This indicates that there is a significant variation expected with results from these tests. This is explained by the large number of variables which are associated with these tests, such as fluctuations in the temperature cycle or the presence of any voids or other flaws in the solder joint which might cause stress concentrations.

The majority of the alloys tested displayed a steady, almost linear decrease in maximum cyclic load with the number of cycles tests. The exceptions to this were Sn-Ag-Bi, Sn-5Sb, and Sn-Pb-5Ni. These three solders had maximum cyclic loads which changed very little with the number of cycles. The area in each hysteresis curve remained almost constant with time for the high melting temperature alloys (Sn-Ag-Bi, Sn-Ag-Bi-In, and Sn-5Sb), as well as for Sn-Pb-5Ni.

AMT FRS, Sn-Pb-2.5 Ag, Sn-Pb-2.5In, AMT 63Sn-37Pb, and HPM 63Sn-37Pb displayed large increases in the areas under the hysteresis curve for the first 20 to 30 cycles, after which the area stabilized for the remainder of the test until near failure. Because the area under the hysteresis curve represents the amount of plastic work deforming the sample, much of the damage for these four alloys probably occurred during the first 30 cycles. It is not clear whether coarsened bands formed quickly in these samples during the first 30 cycles, and thus accumulated the damage. Another possibility is that the plastic damage was initially accumulated by another mechanism, and then coarsened bands formed at the locations of maximum plastic damage. Heterogenously coarsened regions were not apparent in the AMT FRS sample and were observed only slightly for Sn-Pb-2.5In.

Table 4-10. Lifetime results of thermomechanical fatigue tests

composition	cycles to failure	average cycles to failure	maximum load during initial cycle (lbs)	average maximum load in initial cycle (lbs)
AMT 63Sn-37Pb	100	94.4	71.7	82.6
	62		86.9	
	96		91.1	
	146		77.6	
	68		85.5	
HPM 63Sn-37Pb	80	116.0	90.5	93.1
	152		95.6	
IEM 63Sn-37Pb	106	106	116.5	116.5
AMT FRS	73	73	78.0	78.0
63Sn-34.5Pb-2.5Ni	146	173.0	88.1	80.4
	200		72.7	
63Sn-32Pb-5Ni	372	265 +	89.3	89.7
	160 +		90.1	
63Sn-32Pb-5Cu	114	124.0	115.8	105.2
	134		94.6	
63Sn-34.5Pb-2.5In	72	68.0	71.6	89.4
	64		85.9	
63Sn-34.5Pb-2.5Ag	50	53.0	85.2	85.1
	56		85.0	
95Sn-5Sb	282 +	280 +	88.9	92.3
	278 +		95.7	
90Sn-3.2Ag-6.8Bi	164	164	84.0	84.0
86Sn-3Ag-4.2Bi-6.8In	108	108	94.2	94.2

* note: a "+" indicates that the test was a run-on

The remaining solder compositions, Sn-Pb-2.5Ni, Sn-Pb-5Cu, and IEM 63Sn-37Pb, displayed a steady increase in area in the hysteresis curve until a maximum was reached around 80 to 100 cycles. This was followed by a slow drop in the area under the hysteresis curve until failure. This type of behavior indicates that increasing amounts of energy were being dissipated in the sample as plastic work in each cycle.

There may be a correlation between results from low cycle fatigue tests and thermomechanical fatigue results. Baynham found that at a displacement amplitude of ± 1.0 mils (the closest of his testing amplitudes to the displacement of ± 0.7 mils used in thermomechanical fatigue tests in this research), the dispersion strengthened alloys (Sn-Pb-5Ni and Sn-Pb-5Cu) and Sn-5Sb had significantly greater fatigue lifetimes than the Sn-Pb eutectic compositions. The tests conducted at elevated temperatures in this research showed that Sn-Pb-5Ni had the best fatigue resistance at elevated temperatures. The dispersion strengthened alloys also had the longest thermomechanical fatigue lifetimes of the near Sn-Pb eutectic solders. The solid solution strengthened alloys that were tested in thermomechanical fatigue (Sn-Pb-2.5In and Sn-Pb-2.5Ag) had lower

lifetimes than the eutectic alloys, while in low cycle fatigue at room temperature these compositions had higher fatigue resistances. However, Sn-Pb-2.5 In had the lowest fatigue lifetimes at elevated temperatures. This may explain the low thermomechanical fatigue results for the solid solution strengthened alloys.

There may be a relationship between the creep strengths and microhardness values of alloys and thermomechanical fatigue lifetimes. Sn-Pb-5Ni and Sn-5Sb had the best creep resistance of the five compositions tested. These two compositions also had the highest microhardness values of the samples tested. These alloys produced the best thermomechanical fatigue lifetimes.

All three of the eutectic Sn-Pb samples contain cracks in the solder near and parallel to the Cu substrate. These cracks seem to run through a coarsened area which contains larger Pb-rich phases than the solder in the middle of the joint. This heterogenously coarsened region is dissimilar to the coarsening which occurred in the aged sample. The cracks tend to connect voids which exist near the Cu substrate. Sn-Pb-2.5In and Sn-Pb-2.5Ag, the solid solution strengthened alloys, appear to have failed in a similar manner as the eutectic compositions. AMT FRS contained cracks near the Cu substrate, but no observable heterogenously coarsened area.

Two of the dispersion strengthened alloys, Sn-Pb-5Ni and Sn-Pb-5Cu, contained cracks that apparently initiated in the intermetallic layer of the sample. In addition, both samples had areas where two cracks ran parallel to the Cu, with one crack in the solder and the other in the intermetallic layer. Cracks in the Sn-Pb-5Cu also propagated from near the Cu substrate to the middle of the solder joint. Sn-Pb-5Ni had areas in the solder almost 50 μm from the Cu substrate, which EDS showed contained large amounts of Cu, which suggests that these areas contain high concentrations of intermetallics. Unlike the other two dispersion strengthened alloys, Sn-Pb-2.5 Ni contained cracks running through heterogeneously coarsened areas. Similar to the Sn-Pb-5Ni sample, there were regions of high concentrations of Cu almost 50 μm away from the Cu substrate.

Table 4-11 lists some of the measurements made for samples failed in thermomechanical fatigue. The size and volume % values were measured in the middle of the solder joint. Table 4-12 contains a comparison of some of these values to measurements made on as-made samples. Most of the samples experienced a large growth in the size of the intermetallic layer after the fatigue test. It was hard to measure a representative value for the intermetallic thickness of both Sn-Pb-5Ni and Sn-Pb-2.5Ni, due to the Cu-rich areas found away from the Cu substrate in the solder. This might explain the negative changes measured for these two alloys.

All of the samples displayed a significant growth in the size of Pb-rich phases after fatigue, with Sn-Pb-2.5 Ni showing the largest growth. This may be partially due to the sample for this alloy undergoing almost 100 more cycles before failure than the eutectic Sn-Pb samples.

Table 4-11. Measurements from SEM micrographs of samples failed in thermomechanical fatigue

composition	average cycles to failure	intermetallic thickness (μm)	average diameter of Pb-phases (μm)	volume % of Pb-phases	coarsened band?
AMT 63Sn-37Pb	94.4	2.9	2.74	24.9 %	yes
HPM 63Sn-37Pb	116.0	3.8	1.99	29.5 %	yes
IEM 63Sn-37Pb	106	2.7	1.83	32.1 %	yes
AMT FRS	73	6.0	1.96	18.7 %	no
63Sn-34.5Pb-2.5Ni	173.0	10.3	3.61	36.1 %	yes
63Sn-32Pb-5Ni	265 +	16.0	1.85	20.7 %	no
63Sn-32Pb-5Cu	124.0	6.9	1.39	15.5 %	no
63Sn-34.5Pb-2.5In	68.0	4.5	1.37	24.6 %	slightly
63Sn-34.5Pb-2.5Ag	53.0	5.7	1.62	23.2 %	yes
95Sn-5Sb	280 +	7.5			
90Sn-3.2Ag-6.8Bi	164	5.3			

Table 4-12. Comparison of thermomechanically fatigued samples to as-made samples

composition	% difference in intermetallic thickness	% difference in average Pb-rich phase diameter	% difference in average volume % of Pb-rich phases
AMT 63Sn-37Pb	20.8 %	182.3 %	27.5 %
HPM 63Sn-37Pb	52.0 %	131.0 %	31.4 %
IEM 63Sn-37Pb	68.8 %	93.0 %	34.4 %
AMT FRS	93.6 %	95.8 %	-54.0 %
63Sn-34.5Pb-2.5Ni	-57.1 %	581.3 %	70.5 %
63Sn-32Pb-5Ni	-2.4 %	150.1 %	31.9 %
63Sn-32Pb-5Cu	97.1 %	82.4 %	-19.3 %
63Sn-34.5Pb-2.5In	55.2 %	62.9 %	13.3 %
63Sn-34.5Pb-2.5Ag	42.5 %	131.9 %	-3.1 %
90Sn-3.2Ag-6.8Bi	-26.4 %		

Table 4-13 lists where cracks were observed to form and grow for the thermomechanically fatigued samples examined by SEM. Table 4-14 contains measurements taken near the Cu substrate where the coarsen band grows if it is present,

and compares these to similar measurements taken in the middle of the Cu substrates (values from Table 4-11).

All of the Sn-Pb eutectic samples and the solid-solution strengthened alloys contained cracks which seemed to propagate through a coarsened band. Sn-Pb-2.5Ni also contained a coarsened band. The other two dispersion strengthened alloys, Sn-Pb-5Ni and Sn-Pb-5Cu, contained no evidence of a heterogeneously coarsened area, possibly due to the dispersoids restricting the heterogeneous growth of grains. This may have led to the longer lifetimes of the dispersion strengthened alloys. In addition, the Sn-Pb-5Ni alloy showed higher microhardnesses than 63Sn-37Pb. Since dispersion strengthened compositions retain their strengths at elevated temperatures, there should be a smaller differences in strengths at the intermetallic-solder interface than for the eutectic and solid solution solder alloys.

Table 4-13. Crack propagation sites for samples failed in thermomechanical fatigue

composition	alloy type	sites for crack initiation and propagation
AMT 63Sn-37Pb	eutectic Sn-Pb	in coarsened band
HPM 63Sn-37Pb	eutectic Sn-Pb	in coarsened band and at intermetallics-solder interface
IEM 63Sn-37Pb	eutectic Sn-Pb	in coarsened band
AMT FRS	near-eutectic	at intermetallics-solder interface
63Sn-34.5Pb-2.5Ni	dispersion strengthened	in coarsened bands
63Sn-32Pb-5Ni	dispersion strengthened	in intermetallics layer
63Sn-32Pb-5Cu	dispersion strengthened	initiate in intermetallics, propagates at intermetallics-solder interface, then runs through middle of joint
63Sn-34.5Pb-2.5In	solid solution strengthened	in coarsened band and at intermetallics-solder interface
63Sn-34.5Pb-2.5Ag	solid solution strengthened	in coarsened band
95Sn-5Sb	lead free, high melting temperature	at intermetallics-solder interface

At least a 10% increase in the average diameter of Pb phases near the Cu substrate as compared to the middle of joint was observed in 5 out of the 7 samples which contained a coarsened band. Interestingly, all of the samples with coarsened bands also had at least a 10% reduction in the volume percentage of Pb-rich phases near the Cu substrate. This suggests that a Sn-enrichment process is occurring in conjunction with the heterogeneous coarsening near the Cu.

Table 4-14. Measurements near Cu substrate of samples failed in thermomechanical fatigue

composition	coarsened band	near Cu substrate		% differences from middle of same joint to near Cu	
		Pb-rich phase diameter (μm)	volume % Pb-rich phases	in diameter of Pb-rich phases	in volume % of Pb-rich phases
AMT 63Sn-37Pb	yes	3.01	19.7 %	9.8 %	-20.7 %
HPM 63Sn-37Pb	yes	2.07	21.2 %	4.0 %	-28.0 %
IEM 63Sn-37Pb	yes	2.28	19.2 %	24.6 %	-40.2 %
AMT FRS	no	2.07	19.5 %	5.5 %	4.8 %
63Sn-34.5Pb-2.5Ni	yes	4.14	26.8 %	14.7 %	-25.6 %
63Sn-32Pb-5Ni	no	1.96	22.8 %	6.0 %	-9.0 %
63Sn-32Pb-5Cu	no	1.36	15.8 %	-1.7 %	1.8 %
63Sn-34.5Pb-2.5In	slightly	1.40	21.5 %	2.7 %	-12.7 %
63Sn-34.5Pb-2.5Ag	yes	1.62	14.5 %	43.3 %	-37.4 %

Table 4-15 contains measurements obtained through an EDS analysis of the coarsened bands in comparison to the middle of the solder joint for three 63Sn-37Pb alloys. The wt % concentrations of Sn and Pb in Sn-rich grains did not change significantly from Sn grains in coarsened bands to Sn grains in the middle of the joint. Pb-rich grains in the middle of the joint contained higher weight percentages of Sn then Pb grains in the coarsened area. In addition, the coarsened bands showed an average of a 6.7% increase in the wt.% of Sn, as compared to the middle of the joint.

The volume % and weight % of Sn was observed to increase in areas which heterogeneously coarsened, in comparison to areas in the middle of the sample which did not undergo this type of coarsening. There are a few possible explanations for this phenomena. As described previously, the Pb-rich grains are initially supersaturated with Sn. This Sn may diffuse out of the Pb phases into the Sn phases by stress and temperature assisted diffusion during the thermomechanical fatigue cycle. This explains the growth in the volume % of Sn phases in the coarsened band, but does not explain the increase in weight % of Sn.

Additionally, Sn may be diffusing from solder farther away from the Cu substrate, also due to stress and temperature assisted diffusion. Stress concentrations are likely to exist near the intermetallic-solder interface (where the coarsened bands are seen to grow) due to the difference in elastic moduli between these two materials. This would increase the diffusion rates of Sn near the interface.

Table 4-15. EDS analysis of coarsened bands

Change in wt. % Sn of Sn-rich grains from coarsened bands to grains in middle of the joint	
HPM 63Sn-37Pb	3.6 %
AMT 63Sn-37Pb	0.0 %
IEM 63Sn-37Pb	-0.9 %

Change in wt.% Sn of Pb-rich grains from coarsened bands to grains in middle of the joint	
HPM 63Sn-37Pb	16.6 %
AMT 63Sn-37Pb	5.4 %
IEM 63Sn-37Pb	11.2 %

Change in average wt.% Sn from coarsened bands and to the middle of the joint	
HPM 63Sn-37Pb	-6.6 %
AMT 63Sn-37Pb	-6.1 %
IEM 63Sn-37Pb	-7.4 %

The Sn-enrichment of coarsened bands is a feature which was not reported for the coarsened bands researched by Grivas, Frear, Morris, et al. An analysis of some of their micrographs was performed using the NIH Image software and is presented in Table 4-16. All five of the micrographs analyzed displayed a large increase in the diameters of Pb-rich phases in the coarsened band. The four pictures which initially contained lamellar eutectic microstructures, obtained by slowly cooling the solder joint after solidification, did not display any increase in the volume % of Sn-rich phases. The micrograph by Marshall which initially contained a globular microstructure, similar to the structure of samples tested in this research, did show a significant amount of Sn enrichment.

It is possible that the lamellar eutectic microstructure impedes the diffusion of Sn into the coarsened area near the Cu substrate. Unlike the globular structure, there is no easy way for Sn to bypass Pb-rich grains (through which Sn does not diffuse freely) in the regular lamellar structure.

Previous researchers have proposed that cracks initiate in coarsened bands in solder during fatigue due to the relative softness of the coarsened area. The Sn-enrichment observed in this research may accelerate the failure of these samples. At 100 °C, Sn is closer to its melting point (T_H=0.74) than Pb (T_H=0.62). Thus, it is expected that the Sn grains will have worse creep resistance than the Pb grains. If the creep damage that occurs in Sn at this temperature and strain level is from grain boundary sliding or another creep mechanism dependent on the grain size, the creep damage will increase as the Sn

grains coarsen. Because the coarsened area contains a higher weight concentration of Sn than the rest of the solder, creep damage may become concentrated here.

Table 4-16. Analysis of coarsened bands in near-eutectic solders found in the literature

| solder alloy | test type | author | initial microstructure | % difference from middle of joint to near Cu | |
				in diameter of Pb-rich phases	in volume % of Pb-rich phases
60Sn-40Pb	thermal fatigue	Marshall	globular	48.5 %	-27.0 %
63Sn-37Pb	thermal fatigue	Morris, Tribula, Summers, and Grivas	lamellar	51.8 %	2.8 %
60Sn-40Pb	creep	Tribula	lamellar	103.5 %	3.3 %
60Sn-40Pb	thermal fatigue, from 35 °C to 125 °C	Morris and Mei	lamellar	(could not resolve grains)	5.3 %
60Sn-40Pb	thermomechanical fatigue	Morris and Mei	lamellar	46.2 %	-2.6 %

An EDS analysis (see Table 4-15) showed that grains in the Sn-enriched regions become moderately segregated into pure Sn and pure Pb grains. Pure Sn has a different coefficient of thermal expansion and a much larger elastic modulus than pure Pb. Therefore, the temperature fluxes associated with thermomechanical fatigue may create a large amount of strain incompatibility between the purified Sn and Pb phases, which can result in the formation of cavities at their interfaces. These cavities can interconnect to form cracks which would spread throughout the coarsened regions.

5. SUMMARY AND CONCLUSION

Solder in Sn-Pb eutectic, dispersion strengthened, solid solution strengthened, and lead free/high melting temperature compositions was investigated in this research. These alloys were tested in several experiments in a lap shear joint configuration. The purpose of these tests was to determine and explain the thermomechanical fatigue characteristics of the various solder alloys.

The initial microstructure of all of the Sn-Pb based alloys was globular, with Pb-rich phases (supersaturated with Sn) in a Sn matrix. Ternary additions to the eutectic composition resulted in smaller initial Pb-phase sizes. Ternary additions might also lead to lower solder paste wetting properties.

Shear tests were conducted at a displacement rate of 1.67×10^{-6} in/sec at room temperature, 75 °C, and 125 °C. Alloys with higher melting points displayed larger ultimate strengths and ductilities. Sn-Pb-5Ni had one of the larger maximum loads at

room temperature, but average results at elevated temperatures. A large amount of voids were visible in the shear samples.

The use of a diffusion pump (resulting in a higher vacuum) during joint processing was seen to reduce the number of visible voids in the solder joints. Pastes mixed with viscosity controls by IEM, Inc. resulted in superior thermomechanical fatigue results then pastes mixed by hand at Washington University.

Creep results showed that Sn-Pb-2.5 In, AMT 63Sn-37Pb, and HPM 63Sn-37Pb deformed by dislocation climb. The presence of a large threshold stress for Sn-Pb-5Ni was reported at all three temperatures, which indicates that the dispersion strengthening remains effective at elevated temperatures. Sn-Pb-5Ni and Sn-5Sb had significantly greater creep resistances than Sn-Pb-2.5 In, AMT 63Sn-37Pb, and HPM 63Sn-37Pb.

Creep exponents for Sn-Pb-2.5 In, AMT 63Sn-37Pb, and HPM 63Sn-37Pb were decreased by more than 50% when the temperatures were raised from room temperature to elevated temperatures, indicating a change in the dominant damage mechanism. This was supported by SEM work of creep and shear samples of eutectic Sn-Pb. At room temperature these samples contained small cracks throughout the joint interconnecting small voids. At 125 °C, cracks formed at or near the intermetallics-solder interface. An explanation was offered based on the change in elastic modulus and strength of the solder at elevated temperatures. Because intermetallics often retain their properties up to high temperatures, a larger difference in properties exists at the intermetallics-solder interface at elevated temperatures.

Thermomechanical fatigue results are summarized in Table 5-1. The dispersion strengthened and lead free alloys had the longest lifetimes, followed by eutectic Sn-Pb. The solid solution strengthened compositions had the lowest lifetimes.

The formation of a Sn-enriched, coarsened band was observed in the eutectic alloys, in the solid solution strengthened compositions, and in Sn-Pb-2.5 Ni. The Pb grains in this region contained lower weight percentages of Sn than Pb phases in the middle of the solder joint. Cracks were observed to initiate and propagate through this band. The heterogeneously coarsened area was hypothesized to form because of strain and temperature assisted diffusion in stress concentrations near the intermetallics-solder interface. Compositions which contained a Sn-enriched, coarsened bands generally had lower lifetimes.

It was proposed that the Sn-enrichment of coarsened areas contributes to the failure of the solder joint. This was explained by the presumed lower creep resistance of Sn than Pb (Sn has a lower melting point) and to the large difference in physical properties of the Sn and Pb phases.

Table 5-1. Summary of thermomechanical fatigue results

composition	average cycles to failure	composition type	Sn-enriched, coarsened band?
95Sn-5Sb	280 +	lead free, high melting point	no
63Sn-32Pb-5Ni	265 +	dispersion strengthened	no
63Sn-34.5Pb-2.5Ni	173.0	dispersion strengthened	yes
90Sn-3.2Ag-6.8Bi	164	lead free, high melting point	no
63Sn-32Pb-5Cu	124.0	dispersion strengthened	no
HPM 63Sn-37Pb	116.0	eutectic	yes
86Sn-3Ag-4.2Bi-6.8In	108	lead free, high melting point	no
IEM 63Sn-37Pb	106	eutectic	yes
AMT 63Sn-37Pb	94.4	eutectic	yes
AMT FRS	73	near eutectic	no
63Sn-34.5Pb-2.5In	68.0	solid solution strengthened	slightly
63Sn-34.5Pb-2.5Ag	53.0	solid solution strengthened	yes

The dispersion strengthened solders with larger volume fractions of dispersoids (Sn-Pb-5Ni and Sn-Pb-5Cu, but not Sn-Pb-2.5Ni) were effective in impeding the formation of heterogeneously coarsened areas. Cracks were observed to initiate at the intermetallic-solder interface and in the intermetallic layer for these alloys.

Analysis of results from other researchers suggests that the coarsened bands that form in solders which have an initially lamellar microstructure are not Sn-enriched. It was proposed that the lamellar microstructure obstructs the diffusion of Sn into the coarsened area from the bulk solder. An initially globular microstructure in the literature was observed to contain a Sn-enriched coarsened band similar to that seen in this research.

Relations may exist between creep, shear, and isothermal low cycle fatigue results and thermomechanical fatigue lifetimes. Table 5-2 lists the rankings of five alloys in the tests conducted in this research. Shear rankings were based on shear strengths, creep rankings were based on creep resistances, higher microhardness values gave higher rankings, and longer lifetimes in low cycle and thermomechanical fatigue resulted in higher rankings. Sn-Pb-5Ni and Sn-5Sb consistently had the highest rankings in all of the tests. Sn-Pb-2.5In had similar rankings to the two eutectic alloys, except for significantly lower lifetimes in elevated low cycle fatigue tests. HPM 6337 was observed to have slightly better results than AMT 6337. The order for results for thermomechanical fatigue was close to the order of the average rankings for the other tests.

Table 5-2. Relative ranking of various tests

test types	AMT 6337	HPM 6337	Sn-Pb-2.5In	Sn-Pb-5Ni	Sn-5Sb
shear	3	3	3	2	1
creep	3	3	2	1	1
microhardness	4	4	3	2	1
low cycle fatigue:	4	2	3	1	-
room temperature					
75 °C	3	1	4	2	-
125 °C	3	2	4	1	-
average of above	3.3	2.5	3.2	1.5	1
thermomechanical fatigue	4	3	5	2	1

In conclusion, the dispersion strengthened alloys, especially Sn-Pb-5Ni, were observed to have longer thermomechanical fatigue lifetimes than eutectic Sn-Pb solders. This strengthening was attributed to the obstruction to the formation of heterogeneously coarsened regions. Solid solution strengthened alloys had the lowest thermomechanical lifetimes of the alloys tests, possibly due to this type of strengthening not remaining effective at elevated temperatures. The presence of a Sn-enriched coarsened band was observed for the eutectic and solid-solution alloys. Cracks were observed to initiate and propagate through this band.

6. LIST OF PUBLICATIONS AND REPORTS

Steve Baynham, Master of Science thesis: "Mechanical Properties of In-Situ Composite Solder Joints," August 1995.

Brett Goldstein, Master of Science thesis: "Thermomechanical Fatigue of Lap Shear Solder Joints," May 1996.

B. Goldstein, K .L. Jerina and S. M. L. Sastry, "Microstructure Evolution and Thermomechanical Fatigue Life of Solder Joints," submitted to the 29th National Symposium on Fatigue and Fracture.

S. P. Baynham and B. Goldstein, "Producing Quality Lap Shear Solder Joints," in preparation.

B. Goldstein and S. P. Baynham, "Comparison of the Mechanical Properties of Bulk and Single Lap Shear Eutectic Sn-Pb Based Solders," in preparation.

B. Goldstein, "Thermomechanical Fatigue of Sn-Pb Based Lap Shear Solder Joints Part I: Binary Eutectic Alloys," in preparation.

B. Goldstein, "Thermomechanical Fatigue of Sn-Pb Based Lap Shear Solder Joints Part II: Ternary Alloys," in preparation.

7. LIST OF PARTICIPATING PERSONNEL

1 Sep 92 to 31 Dec 92
    Jon Albee, Graduate Student
1 Jan 93 to 30 Jun 93
    Steve Baynham, Graduate Student
    Mary Kerr, Graduate Student
1 Jul 93 to 31 Dec 93
    Steve Baynham, Graduate Student
1 Jan 94 to 30 Jun 94
    Steve Baynham, Graduate Student
1 Jul 94 to 31 Dec 94
    Steve Baynham, Graduate Student
1 Jan 95 to 30 Jun 95
    Steve Baynham, Graduate Student
    Brett Goldstein, Graduate Student
1 Jul 95 to 31 Dec 95
    Steve Baynham, Graduate Student, Master of Science, May 1995
    Brett Goldstein, Graduate Student
1 Jan 96 to 31 Aug 96
    Brett Goldstein, Graduate Student, Master of Science, May, 1996

8. INVENTIONS

There were no inventions or patents issued as a result of this work.

9. REFERENCES

1.   Morris, J.W., D. Grivas, D. Tribula, T. Summers, and D. Frear. 1989. Research on the Mechanism of Thermal Fatigue in Near-Eutectic Pb-Sn Solders. *Soldering & Surface Mount Technology* 3: 25-32.
2.   Frear, D.R., M.M. Rashed, S.N. Burckett. 1993. Microstructurally Based Thermomechanical Fatigue Lifetime Model of Solder Joints for Electronic Applications. *Reliability, Stress Analysis, and Failure Prevention* 55: 171-180.
3.   Jahsman, W.E., P. Jain, D.E. Pope, and K. Byrd. 1991. Measurement and Modeling of In Situ Lead Stiffness of Surface Mounted Packages. *IEEE Transactions on Components, Hybrids, and Manufacturing Technology* 14: 859-69.
4.   S.M.L. Sastry, D.R. Frear, C.G. Kuo, and K.L. Jerina. 1993. The Properties of Composite Solders. In *The Mechanics of Solder Alloy: Wetting and Spreading*, eds. F.M. Hosking and D.R. Frear, 299-352. New York: Van Nostrand Reinhold.

5.   J.K. Tien, B.C. Hendrix, A.I. Attarwala. 1991. The Interaction of Creep and Fatigue in Lead-Tin Solders. In *Solder Joint Reliability*, ed. J.H. Lau, 279-304. New York: Van Nostrand Reinhold.

6.   Morris, J.W. and Z. Mei. 1991. Toward New Solders with Improved Fatigue Resistance. In *Solder Mechanics: A State of the Art Assessment*, eds. D.R. Frear, W.B. Jones, and K.R. Kinsman, 239-70. Warrendale, PA: TMS Publications.

7.   Karakaya, I. and Thompson, W. T., *Bull. Alloy Pha. Dia.*, 1988, Vol. 9, pp144-152.

8.   Frear, D.R. 1991. Thermomechanical Fatigue in Solder Materials. In *Solder Mechanics: State of the Art Assessment*, eds. D.R. Frear, W.B. Jones, and K.R. Kinsman, 191-237. Warrendale, PA: TMS Publications.

9.   Roeder, J.F., M.R. Notis, and H.J. Frost. 1991. Physical Metallurgy of Solder Systems. In *Solder Mechanics:A State of the Art Assessment*, eds. D.R. Frear, W.B. Jones, and K.R. Kinsman, 1-27. Warrendale, PA: TMS Publications.

10.   Tribula, D., D. Grivas, D.R. Frear, and J.W. Morris. 1989. Microstructural Observations of Thermomechanically Deformed Solder Joints. *Welding Research Supplement* 404-9.

11.   Morris, J.W., D. Tribula, T.S.E. Summers, and D. Grivas. 1991 The Role of Microstructure in Thermal Fatigue of Pb-Sn Solder Joints. In *Solder Joint Reliability*, ed. J.H. Lau, 225-65. New York: Van Nostrand Reinhold.

12.   R. Arrowood, A. Mukherjee, and W.B. Jones. 1991 Hot Deformation of two-Phase Mixtures. In *Solder Mechanics:A State of the Art Assessment*, eds. D.R. Frear, W.B. Jones, and K.R. Kinsman, 107-53. Warrendale, PA: TMS Publications.

13.   Evans, J.W., J.Y. Evans, and S.M Hull. The Effects of Cerium and Silver Alloying on Microstructure and Fatigue in Near Eutectic Solders. 739-57.

14.   Honeycomb, R.W.K. 1968. *The Plastic Deformation of Metals.* New York: St. Martin's Press.

15.   Clough, R.B., A.J. Bayba, A.J. Shapiro, and G.K. Lucey. 1993. Boundary Layer Fracture of Copper/Composite Solder Interfaces. *First ASME International Electronic Packaging Conference*, ed. P. Engel.

16.   Roming, A.D., Y.A. Chang, J.J Stephens, D.R. Frear, V. Marcotte, and C. Lea. 1991. Physical Metallurgy of Solder-Substrate Reactions. In *Solder Mechanics:A State of the Art Assessment*, eds. D.R. Frear, W.B. Jones, and K.R. Kinsman, 29-104. Warrendale, PA: TMS Publications.

17.   Kuo, C.G. 1994. Creep-Fatigue Interactions in Eutectic Tin-Lead-Based Solder Alloys. Ph.D. diss, Washington University.

18.   Smithells, C.J. *Smithells Metal Reference Book*, ed. E.A. Brandes and G.B. Brook, 1992. Oxford, Boston: Butterworth-Heinemann.

19.   Pinizzotto, R.E., Y. Wu, E.H. Jacobs, and L.A. Foster. 1992. Microstructural Development in Composite Solders Caused by Long Time, High Temperature Annealing. Proc. of Tech Prog NEPCON West '92, 3: 1284-98.

20.   Frear, D., D. Grivas, and J.W. Morris. 1989. A Microstructural Study of the Thermal Fatigue Failures of 60Sn-40Pb Solder Joints. *Journal of Electronic Materials* 17: 171-80.

21.   Z. Guo, P. Hacke, A.F. Sprecher, and H. Conrad. Effect of Composition on the Low-Cycle Fatigue of Pb Alloy Solder Joints. IEEE.

22. Darveaux, D. and K. Banerji. 1992. Constitutive Relations for Tin-Based-Solder Joints. *IEEE Transactions on Components, Hybrids, and Manufacturing Technology* 15: 1013-24.

23. Akay, H.U., Y. Tong, and N. Paydar. Thermal Fatigue Analysis of an SMT Solder Joint Using Nonlinear FEM Approach.

24. Baynham, S. 1995. Mechanical Properties of In-Situ Composite Solder Joints. M.S. thesis, Washington University.

25. Holford, G.R., B.A. Lerch, J.F. Saltamar, and V.K. Arya. 1993. Proposed Framework for Thermomechanical Fatigue (TMF) Life Prediction of Metal Matrix Composites. In *Thermomechanical Fatigue Behavior of Materials*, ASTM STP 1186, ed. H. Lehitoglu, 50-69. Philadelphia: American Society for Testing and Materials.

26. Majumdar, S. and W.B. Jones. 1991. How Well Can We Predict the Creep-Fatigue Life of a Well-Characterized Material?. In *Solder Mechanics:A State of the Art Assessment*, eds. D.R. Frear, W.B. Jones, and K.R. Kinsman, 273-360. Warrendale, PA: TMS Publications.

27. Bannantine, J.A., J.J Comer, and J.L. Handrock. 1990. *Fundamentals of Metal Fatigue Analysis*. Englewood Cliffs, NJ: Prentice Hall.

28. Courtney, T.H. 1990. *Mechanical Behavior of Materials*. New York: McGraw-Hill Publishing Co.

29. Reed-Hill, R.E. 1973. *Physical Metallurgy Principles*. 2nd ed. Boston: PWS-Kent Publishing Co.

30. Sastry, S.M.L., T.C. Peng, R.J. Lederich, K.L Jerina, and C.G. Kuo. 1992. Microstructures and Mechanical Properties of In-Situ Composite Solder. Proc. NEPCON '92, 3: 1266-75.

31. Hwang, J.S. and Z. Guo. 1994. Lead-Free Solders for Electronic Packaging and Assembly. *Circuit World* 20: 19-25.

32. Wong, B., C.A. Megerle, D.L. O'Brien, W.E. Elias, W.R. Gesick, and D.B. McKerman. Fatigue-Resistant Solder.

33. Vaynmar, S. and M.E. Fine. 1991. Effects of Strain Range, Ramp Time, Hold Time, and Temperature on the Isothermal Fatigue of Tin-Lead Solder Alloys. In *Solder Joint Reliability*, ed. J.H. Lau, 333-57. New York: Van Nostrand Reinhold.

34. Frear, D.R., W.B. Jones, and N.E. Sorensen. 1992. Hold Time, Strain Rate, and the Environmental Effects of Near Eutectic Sn-Pb Solder Under Conditions of Thermomechanical Fatigue. Proc. of the 5th Conference on Creep of Materials, Lake Buena Vista, FL.

35. Frear, D.R., N.R. Sorensen, J.S. Martes. 1994. Test Methodologies to Perform Valid Accelerated Thermomechanical Fatigue Tests of Solder Joints. In *Fatigue of Electronic Materials*, ASTM STP 1153, eds. S.A. Schroeder and M.R. Mitchell, 95-109. Philadelphia: American Society for Testing and Materials.

36. Engelmaier, W. Design for Reliability for Surface Mount Solder Attachments: Physics of Failure and Statistical Failure Distributions.

37. Shine, M.C. and L.R. Fox. 1988. Fatigue of Solder Joints in Surface Mount Devices. In *Low Cycle Fatigue*, ASTM STP 942, eds. H.D. Solomon, G.R. Halford, L.R. Kaisand, and B.N. Leis, 588-610. Philadelphia: American Society for Testing and Materials.

38.   Kilinski, T.J., J.R. Lesniak, and B.I. Sandor. 1991. Modern Approaches to Fatigue Life Prediction of SMT Solder Joints. In *Solder Joint Reliability*, ed. J.H. Lau, 384-405. New York: Van Nostrand Reinhold.

39.   Solomon, H.D. 1991. Predicting Thermal and Mechanical Fatigue Lives from Isothermal Low Cycle Data. In *Solder Joint Reliability*, ed. J.H. Lau, 406-54. New York: Van Nostrand Reinhold.

40.   Wood, N.O. 1992. Predicting SMT Solder Joint Reliability Using Calculated Temperatures. *Electronic Packaging and Production*, 72-4.

41.   Hall, P.M. 1991. Creep and Stress Relaxation in Solder Joints. In *Solder Joint Reliability*, ed. J.H. Lau, 306-32. New York: Van Nostrand Reinhold.

42.   Johnson, C.C. and J. Kevra. 1989. *Solder Paste Technology*: Principles and Applications. Blue Ridge Summit, PA: TAB Professional and Reference Books.

43.   O'Hara, W.B. and N. Lee. 1996. How Voids Develop in BGA Solder Joints. *Surface Mount Technology* 10: 44-7.